Iraqi Geological Journal

Journal homepage: https://www.igj-iraq.org

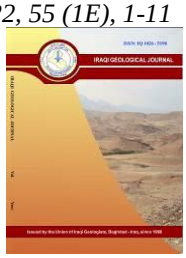

Metamorphic Evolution of the Bulfat Belt (NE-Iraq): Evidence from $^{40}Ar/^{39}Ar$ Age Spectrum Measurements

Elias M. Elias[1], Zahraa J. Al-Jubory [1,*] and Ahmed M. Aqrawi [2]

[1] Department of Geology, College of Science, Mosul University, Mosul, Iraq
[2] Department of Geology, College of Science, Salahaddin University, Erbil, Iraq
* **Correspondence**: zahraa1981@uomosul.edu.iq

Received:
6 October 2021

Accepted:
26 August 2022

Published:
31 May 2022

Abstract

The Bulfat Ophiolite Complex (upper allochthonous thrust sheet) which represents a part of the Iraqi Zagros Suture Zone is situated at the boundary between the Arabian Plate and the Iranian Microplate. We have examined the metamorphic and cooling history of metapelitic rocks of Bulfat Complex using the whole-rocks $^{40}Ar/^{39}Ar$ age determination. The results of four samples match to the definition of the plateau and revealed to 40Ar/ 39Ar age of 42.4 ±0.5 Ma (sample 1), 32.9 ±0.8 Ma (sample 2), 44.3 ±0.8 Ma (sample 3), and 43.6 ±1.5 Ma (sample 5). However, samples 4 and 6 yielded an age range between 35- 40 Ma and 40- 50 Ma respectively. Generally, plateau ages (32.9-50 Ma) are identical and considered reliable, but the presence of excess argon (^{40}Ar) remains possible in samples (e.g., sample 6) having initial $^{40}Ar/^{36}Ar$ ratios higher than the present atmospheric $^{40}Ar/^{36}Ar$ = 295.5. The excess argon is derived from the mantle by plumes of mafic magmas into the earth crust and/ or released from minerals and rocks during metamorphic processes. Bulfat Complex is subjected to two metamorphic events: the earlier regional occurred during the period Albian-Cenomanian (97-105 Ma) and associated with the intraoceanic infant supra-subduction zone. The later thermal metamorphism overprinted the previous one, and took place due to the intrusion of igneous body pre – 50 Ma age. This igneous activity is considered one of the multi-event magmatism that happened along the Zagros Fold-Thrust Belt during the period from Upper Cretaceous and Mid – Late Miocene. It seems evident that the thermal metamorphic slice of Bulfat Complex (Gemo-Qandil Sequence) represents a part of the oceanic slab that has been subducted beneath the Iranian microplate. This event probably forming the last evolved episode of island arc system ended with the final closure of Neo-Tethys and the collision between the Arabian Plate and Iranian Microplate occurred at Mid-late Miocene.

Keywords: Zagros Suture Zone; Bulfat complex; Thermal metamorphism; 40Ar/39Ar age; Neo-Tethys

1. Introduction

Application of $^{40}Ar/^{39}Ar$ step-heating in metamorphic belts can provide information on the timing of metamorphism and/or post-metamorphic uplift and cooling events. Argon may diffuse from minerals

DOI: 10.46717/igj.55.1E.1Ms-2022-05-17

by heating or may be lost during recrystallization processes that accompany thermal overprinting events (Wijbrans and McDougall, 1988). Thus, accurate evaluation of $^{40}Ar/^{39}Ar$ ages of crustal rocks in terms of the thermal evolution of crustal rocks requires precise knowledge of the mineral content of the measured sample as well as the P-T conditions experienced by the system during metamorphism. The quantitative accumulation of radiogenic argon within k-bearing minerals whether coincide with certain metamorphic conditions or occurs after the cooling of minerals below their closure temperatures remains a matter of debate.

The Bulfat complex is situated at the boundary between the Arabian Plate and the Iranian microcontinent that represents a part of ZSZ. The complex together with Mawat and Penjween complexes belongs to the upper allochthonous thrust sheets (Gemo-Qandil sequence) that formed in the Neo - Tethys Ocean during Albian- Cenomanian (Aswad and Elias,1988; Aswad et al., 2011). The complexes were thrust above the passive margin of the Arabian Plate as two distinct stages of subduction, and the collision happened during the period Late Cretaceous –Late Miocene (Jasim and Buday, 2006; Aziz et al., 2011). The lower allochthonous thrust sheet comprises the Walash Volcano-Sedimentary rocks intertwined with Naopurdan sedimentary group (Aswad, 1999; Aswad, et al., 2011). Referring to the previous studies Bulfat complex is subjected to at least two types of older and younger intrusions. The older is composed mainly of gabbro and diorite while the younger smaller intrusion is composed of olivine gabbro- diorite (Jasim and Buday, 2006). The volcano-sedimentary succession in the Bulft complex is regionally metamorphosed. The regional metamorphic condition of Bulfat complex is of the low grade under conditions of greenschist–the onset of the amphibolite facies (Jasim et al., 2006). Regionally metamorphosed rocks of the Bulfat complex were affected by many pulses of strongly differentiated gabbros forming a wide metamorphic aureole of up to 2.5 Km around the igneous intrusions. The contact metamorphic zones of the Bulfat country rocks are composed of sanidinite facies, pyroxene hornfels facies, hornblendite hornfels facies, and albite-epidote hornfels facies (Aswad and Pashdari,1984; Jassim et al., 2006; Elias and Al-Jubory, 2013). The latter facies pass into greenschist regional metamorphic facies of the Bulfat group. Because the Bulfat complex was subjected to contact metamorphism, it can be assumed that the apparent $^{40}Ar/^{39}Ar$ age of bulk samples is a reasonable approximation of the late contact metamorphic event. Furthermore, the petrology of the rocks allows an estimate of P-T conditions (Elias and Al- Jubory, 2013). In the present paper, an attempt is made to evaluate the $^{40}Ar/^{39}Ar$ age spectrum of six metapelitic samples to gain complementary insight into the thermal–tectonic evolution of the Bulfat metamorphic belt.

2. Geological Background

The research area (Fig. 1) is located along the Iraqi-Iranian–Turkish boundaries and was formed as a result of the Arabian Plate margin colliding with Iranian Microplates accompanied the closure of Neo-Tethys (Alavi, 2004; Aziz et al., 2011; Aswad et al., 2011). The Bulfat complex is a part of the Iraqi Zagros dismembered ophiolite sequence that occupies 100Km^2 cropping out in Bulfat mountain near Qlala-Dizeh town, NE Iraq.The metapelite rocks that are the subject of this study situated in Bulfat Mountain in NE Iraq, at an elevation of 1659 meters. samples had been collected from Qandil group between longitudes (45° 16’972” –45° 16’ 884” E) and latitudes (36° 11’322”- 36°11’ 302” N) about 65 Km. from north of Qala-Dizeh town. These metapelites were a part of the metasedimentary group of Qandil sequences which are calcsilicates, carbonate sand metavolcanic that formed in early-Cretaceous and then regionally metamorphosed.

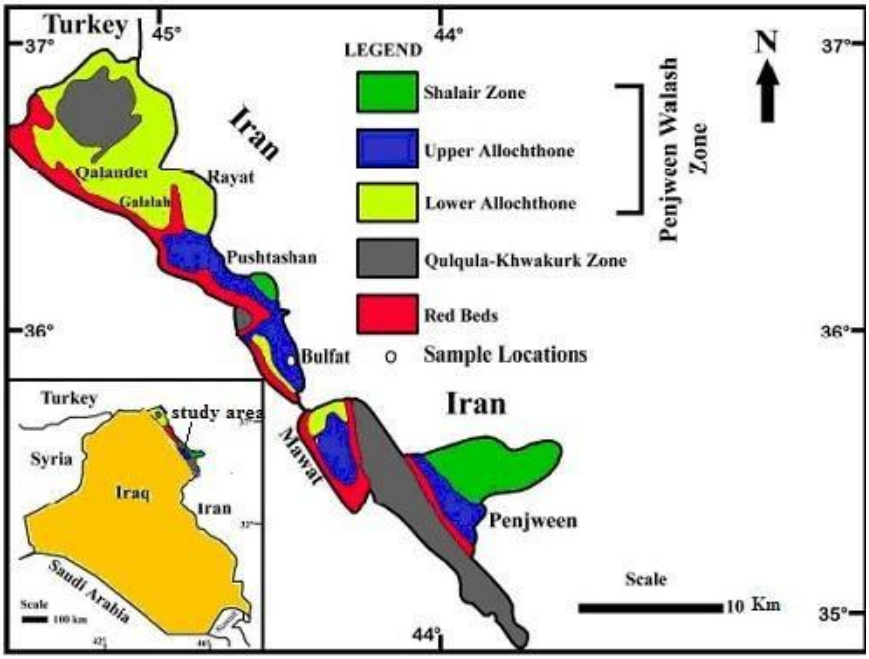

Fig. 1. Simplified geological map showing the studied area (Aziz, 2008)

During the regional metamorphic event, no changes were noticed in terms of the textures and chemical characteristics of protolith rocks. These rocks were strongly subjected to thermal metamorphism due to gabbro intrusive body formed a wide metamorphic aureole of about 2.5Km. Contact metapelitic rocks in the Bulfat complex were identified (Elias and Al- Jubory, 2013) as hornfels with characteristic mineral assemblages of Cordierite + Fibrolite + Andalusite + Muscovite + Biotite + Feldspar+ Quartz, and Cordierite + Fibrolite +Biotite+ Muscovite + Feldspar + Quartz. In this regard, the hornfels rocks were distinguished by their fine-grained minerals and various textures, including granoblastic, porphyroblastic, poikiloblastic, and intergrowth (Fig.2). The effect of deformation was noticed mainly in biotite and fibrolite (Fig.2 a), probably due to the later thrusting process. P-T estimation of hornfelsic rocks indicates a temperature reached up to ~ 668Co and pressures 2.9 Kbar-3.5 Kbar corresponding to hornblende hornfels- the beginning of pyroxene hornfels facies. Metapelites were then probably affected by a process of exhumation and cooling at a temperature of about 581Co and pressure about 2Kbar (Elias and Al-Jubory, 2013).

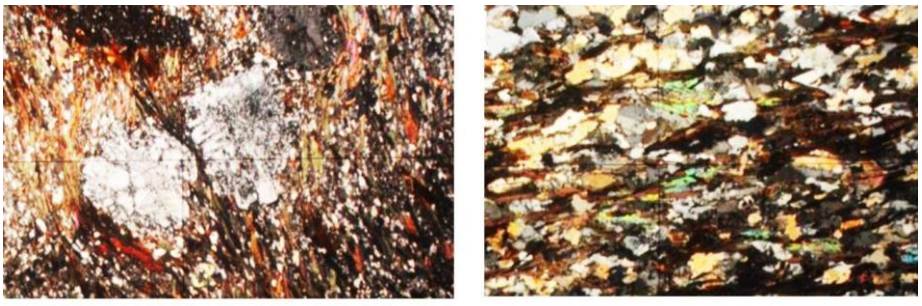

(a) (b)

Fig. 2. A) Porphyroblastic texture of metapelites rocks (sample 1); B) Granoblastic texture of metapelites rocks (sample 3)

Geochemical investigation of metapelites (Al-Jubory, 2011) indicates their enrichment in light rare-earth elements (LREE), large ion lithophile elements (LILE), and relative depletion in high- field strength elements (HFSE). These characteristics with a prominent -ve Eu anomaly (Eu/Eu* =0.56- 0.81) are similar to the average Eu/Eu* value of Post- Archean Australian Shale (PAAS) and upper continental crust (UCC), UCC (Eu/Eu* =0.65, Mclennan, 1989). Therefore, sediments may have been originally derived from upper continental crust that was mostly felsic in composition.

3. Experimental Technique

Six whole-rock samples were crushed and sieved to identify the age of igneous intrusion and the associated metamorphic pelitic rocks. 40Ar/39Ar dating on metapelites enriched with K -bearing minerals (biotite, muscovite, and relatively less K-feldspar) can provide important constraints on the timing of medium to high temperature and relatively low-pressure contact metamorphism. Step-heating spectra based on the implied initial 40Ar/39Ar composition for four samples (1, 2, 3, 5) record well-defined and concordant plateau ages (32.9-44.3Ma) suggesting that obtained ages are not affected by excess argon, and /or post crystallization diffusive loss of radiogenic argon. Matrix (groundmass) samples were picked from the 250-500-micrometer fraction to avoid large visible crystal inclusion. Samples were irradiated at the USGS Triga reactor in Denver (USA) with an irradiation time of 10 hours. To establish a J-value for the age calculation, the samples were co-irradiated with 4 fish Canyon sanidine monitor standards. We used the 28.02 Ma age for this standard to calculate J-values (Renne et al., 1998). The LDEO Ar lab is equipped with a fully custom constructed and automated micro-extraction equipment as well as a VG5400 mass spectrometer for measuring 40Ar-39Ar of samples. Coaxial CO2 and UV lasers, as well as a video camera and a Newport X-Y-Z stage, make up the laser and beam delivery system. The system is entirely automated, and the vacuum valves are controlled by pneumatically driven valves that are achieved by electro-pneumatic solenoid valves. Gases released from the heating of samples are scrubbed of reactive gases such as H_2, CO_2, CO, and N_2 by exposure to Zr - Fe-V and Zr-Al sintered metal alloy getters. The inert gases, primarily Ar, are then fed into the mass spectrometer, where the Ar-isotopic ratios are calculated using Al Deino's Berkeley Geochronology Center's data software.

A modified Nier ion source and a 90° sector extended-geometry are used in the LDEO Ar mass spectrometer. In static mode, the mass spectrometer is used. For both the extraction system and the mass spectrometer, M/e 36 cold procedure blanks are less than 5 x 10-14 cc STP. The desorption of ^{40}Ar in the vacuum envelope's stainless-steel wall is less than 1 x 10-12 cc STP/min. The VG 5400 has a detection limit of around 1 x 10-14 cc STP (about 5 x 10-19 moles) or about 1 x 10-3 Amps/Torr at 200 mA trap current. Monitor standards were fused in a single step at 7 Watts with a CO_2 laser. Samples were step-heated with progressively higher Watts with a CO_2 laser (values of the heating steps are reported in the data tables). During the runs of the samples and monitors, blanks and air pipette standards were run frequently. Reported data are corrected for background based on blank runs and for mass discrimination based on air pipette standards. They are also corrected for nuclear interferences using reported data (Mick Kunk, USGS Ar geochronologist, personal communication).

4. Results and Discussion

Six samples were collected from different locations covering a distance of ~170 meters from the contact of the basic igneous body. The results of the analyses are reported in Table 1 and are presented as step heating spectra and isochrons (Fig. 3). The definition we used for plateaus is that they must

include at least 3 steps and 50% or more of the total ^{39}Ar released. The reported plateau ages are weighted by precision, and the integrated ages are weighted by gas content. Amongst the samples, four

of the six samples conformed to the definition of the plateau and reveal $^{40}Ar/^{39}Ar$ plateau ages of 42.4± 0.5 Ma (sample 1), 32.9± 0.8 Ma (sample 2), 44.3±0.8Ma (sample 3), and 43.6±1.5Ma (sample 5). However, samples 4 and 6 yielded age range between 35-40 Ma and 40- 50Ma respectively. Inverse isochron plots of the present samples display identical ages within errors to the respective plateau ages (Table 1 and Fig. 3). This is in spite of the different initial ratios of $^{40}Ar/^{36}Ar$ (250– 470). Thus, Plateau ages (32.9–50 Ma) can be considered reliable, but the presence of excess argon ($^{40}Ar^*$) remains possible in samples having initial $^{40}Ar/^{36}Ar$ ratios higher than the present atmospheric $^{40}Ar/^{36}Ar$ ratio (295.5). It is known that excess argon is derived from the mantle by plumes of mafic magmas into the earth's crust (Dalrymple, 1991). In addition to the primordial 40Ar from the mantle, there is a radiogenic argon $^{40}Ar^*$ that may have been released from minerals and rocks during diagenesis and metamorphism processes. Thus, continued migration and circulation of both types of released argon remain possible in samples of crustal rocks that reflect their presence in CO_2 enriched natural gases. The age spectrum of sample 1 shows an excellent plateau age (42.4±0.5 Ma) over almost 90% of the ^{39}Ar released (Fig. 3, A). This plateau age is identical to the integrated age (42.4±1.6Ma) as well as to the isochron age (42.4±0.3Ma), (Fig. 3 a) when regressed in terms of $^{39}Ar/^{40}Ar$ versus $^{36}Ar/^{40}Ar$ despite the higher initial 40Ar/36Ar value of 350±10 than the presumed value for atmospheric argon, 295.5. Sample 2 yielded a concordant spectrum with an integrated age of 32.9±0.8 Ma (5 steps; Fig. 3B) over ~ 65% of the ^{39}Ar released. This age is remarkably consistent with the isochron age of 32.9±1.0 Ma (Fig.3b). Sample 3, however, revealed an excellent age spectrum with a plateau age of 44.3±0.8 Ma (5 steps; Fig. 3C) over ~94% of the ^{39}Ar released, excluding the last step of the discordant age spectrum (~ 75 Ma) at high temperature degassing which is accompanied by elevated Ca/K. Additionally, the age is consistent (within the errors) with both integrated age (46.0±1.5Ma) and isochron age of 44.3±1.2 Ma (Fig. 3C).

Excluding the first step of heating, the profound plateau age of 43.6±1.5 Ma (5 steps; Figure 3, E including ~ 92% of the ^{39}Ar released) recorded in the age spectrum of sample 5 seems to be comparable with the age 44.3±0.8 Ma obtained by sample 3. In this concern, the plateau age of sample 5 corresponds (within the errors) to the isochron age of 43.6±1.9 Ma (Fig. 3 e) and with a lesser extent, to the integrated age of (37±5 Ma). The age spectra of samples 4 (Fig. 3d) and 6 (Fig. 3e) are similar in appearance as their apparent ages in the low extraction temperatures (over ~ 40% of the ^{39}Ar released) are fluctuated and poorly constrained in agreement with variable values of Ca/K. In this context, low and variable apparent ages in the initial steps of extraction may be related to episodic loss of radiogenic argon from the mineral systems and/or excess ^{40}Ar that were incorporated subsequent to the beginning of argon accumulation. However, age spectra of samples 4 and 6 at higher temperatures over ~ 60% of the ^{39}Ar released may be significant, reflecting two distinct plateaus characterized by age range 35–40 Ma (Sample 4) and 40–50Ma (Sample 6).

Table 1. $^{40}Ar/^{39}Ar$ analytical data of metapelites from Bulfat complex.

Sample 1 (J = 0.002198 ± 0.000001)													
Run ID	**Status**	**Watts**	**Ca/K**	**Cl/K**	**36Ar/39Ar**	**%36Ar(Ca)**	**40*Ar/39Ar**	**Mol 39Ar**	**% Step**	**Cum. %**	**%40Ar***	**Age (Ma)**	**± Age**
•13302-01A	OK	0.1	0.1935954	0.0061783	0.0468199	0	13.18529	1.44E-14	17.9%	17.9%	48.7974	51.54113	1.833749
•13302-01B	OK	0.3	0.1472439	0.0086347	0.0108538	0	11.39302	4.19E-15	5.2%	23.1%	78.0335	44.62107	0.8886591
•13302-01C	OK	0.6	0.1335055	0.0095861	0.0049767	0	10.99255	5.98E-15	7.4%	30.5%	88.2016	43.07117	0.6452332
•13302-01D	OK	1	0.1182556	0.0084101	0.0098132	0	11.28857	1.05E-14	13.1%	43.6%	79.5629	44.21694	0.6655661
•13302-01E	OK	3	0.1527396	0.0030053	0.0075914	0	11.45403	2.37E-14	29.5%	73.2%	83.6229	44.85706	0.548572
•13302-01F	OK	7	0.1575059	0.0045269	0.0011198	0	10.86301	2.16E-14	26.8%	100.0%	97.0446	42.56954	0.345306
Integrated Age =												42.4	1.6
(•) Plateau Age =												**42.4**	**0.5**
Sample summary	ID	Irrad.	Material	Integ. Age	Error	% Rad	Age	Error	MSWD	Prob.	Steps	n/n-total	% Gas
Sample 1	13302	USGS8D	Groundmass	42.4	1.6	74.8	**42.4**	**0.5**	0.54	0.75	A,B,C,D,E,F	6/6	100
Sample 2 (J = 0.002198 ± 0.000001)													
13303-01A	OK	0.1	0.1020651	0.005041	0.0186951	0	7.913288	1.42E-14	35.5%	35.5%	58.8892	31.10928	0.8227108
•13303-01B	OK	0.3	0.1035642	0.0069303	0.0039475	0	9.26271	3.21E-15	8.0%	43.5%	88.8162	36.36109	0.8168886
•13303-01C	OK	0.6	0.0741979	0.0064275	0.0057739	0	9.02401	4.70E-15	11.7%	55.2%	84.1001	35.43321	0.6474422
•13303-01D	OK	1	0.0357366	0.0008706	0.0046245	0	9.130421	4.39E-15	10.9%	66.1%	86.9816	35.84692	0.7681505
•13303-01E	OK	3	0.1264401	0.002425	0.0050331	0	9.145665	1.21E-14	30.1%	96.3%	86.0128	35.90617	0.4720026
•13303-01F	OK	7	1.179841	-0.01575	0.0222556	0	11.85762	1.50E-15	3.7%	100.0%	64.3232	46.41744	1.981788
Integrated Age =												28.4	1.5
(•) Plateau Age =												**32.9**	**0.8**
Sample summary	ID	Irrad.	Material	Integ. Age	Error	% Rad	Age	Error	MSWD	Prob.	Steps	n/n-total	% Gas
Sample 2	13303	USGS8D	Groundmass	28.4	1.5	74.0	**32.9**	**0.8**	0.49	0.74	B,C,D,E,F	5/6	65
Sample 3 (J = 0.002198 ± 0.000001)													
•13304-01A	OK	0.1	0.0875102	0.0031696	0.02665	0	9.973557	1.17E-14	27.8%	27.8%	55.8787	39.1215	1.343662
•13304-01B	OK	0.3	0.0786862	0.0105818	0.0102857	0	10.53201	3.23E-15	7.7%	35.5%	77.6054	41.28717	2.729404
•13304-01C	OK	0.6	0.067019	0.0021494	0.0113288	0	11.19852	2.97E-15	7.0%	42.5%	76.9862	43.86847	1.841926
•13304-01D	OK	1	0.0496755	0.001478	0.006264	0	10.51769	5.36E-15	12.7%	55.3%	85.0349	41.23166	1.054115
•13304-01E	OK	3	0.0802318	0.0048457	0.0070613	0	11.18654	1.61E-14	38.3%	93.5%	84.28	43.82211	0.6018891
13304-01F	OK	7	0.3877241	0.002119	0.0055524	0	18.73506	2.73E-15	6.5%	100.0%	91.9478	72.80237	2.688012
Integrated Age =												46.0	1.5
(•) Plateau Age =												**44.3**	**0.8**
Sample summary	ID	Irrad.	Material	Integ. Age	Error	% Rad	Age	Error	MSWD	Prob.	Steps	n/n-total	% Gas
Sample 3	13304	USGS8D	Groundmass	46.0	1.5	74.7	**44.3**	**0.8**	1.96	0.10	A,B,C,D,E	5/6	93.5

Table 1: Continued

Sample 4 (J = 0.002198 ± 0.000001)													
Run ID	**Status**	**Watts**	**Ca/K**	**Cl/K**	**36Ar/39Ar**	**%36Ar(Ca)**	**40*Ar/39Ar**	**Mol 39Ar**	**% Step**	**Cum. %**	**%40Ar***	**Age (Ma)**	**± Age**
13305-01A	OK	0.1	0.0801522	0.006241	0.0386271	0	8.33093	8.49E-15	13.2%	13.2%	42.1923	32.73633	1.543529
13305-01B	OK	0.3	0.0973826	0.0012563	0.0076622	0	9.87437	5.72E-15	8.9%	22.1%	81.3473	38.73659	0.8411498
13305-01C	OK	0.6	0.1168426	0.0052107	0.0072366	0	9.270869	7.48E-15	11.7%	33.8%	81.258	36.3928	0.6693286
13305-01D	OK	1	0.0838424	0.0089396	0.0044707	0	9.785061	5.09E-15	7.9%	41.7%	88.1061	38.38993	0.8480132
13305-01E	OK	3	0.0519431	0.0043843	0.0041603	0	10.20248	1.44E-14	22.4%	64.1%	89.2468	40.00957	0.4852881
13305-01F	OK	7	0.0536007	0.0035419	0.0060118	0	9.179586	2.30E-14	35.9%	100.0%	83.786	36.03803	0.4767276
Integrated Age =												38.6	1.1
Approximate Age Range (no plateau) =												**35-40**	
Sample summary	ID	Irrad.	Material	Integ. Age	Error	% Rad	Age	Error	MSWD	Prob.	Steps	n/n-total	% Gas
Sample 4	13305	USGS8D	Groundmass	38.6	1.1	76.0	**35-40**	N/A	N/A	N/A	N/A	N/A	N/A
Sample 5 (J= 0.002198 ± 0.000001)													
13307-01A	OK	0.1	0.0476216	0.0055541	0.2327201	0	30.38077	4.40E-15	7.9%	7.9%	30.6414	116.6189	8.242643
•13307-01B	OK	0.3	0.0561138	0.0067851	0.0828085	0	22.47368	4.12E-15	7.4%	15.3%	47.8739	86.98512	4.13805
•13307-01C	OK	0.6	0.1004399	0.0095205	0.047456	0	19.27992	6.08E-15	10.9%	26.3%	57.8925	74.8763	2.654731
•13307-01D	OK	1	0.0477942	0.0068909	0.0565063	0	22.34361	2.38E-15	4.3%	30.6%	57.231	86.49355	5.039263
•13307-01E	OK	3	0.1417585	0.0056485	0.0244995	0	16.30131	1.68E-14	30.3%	60.9%	69.247	63.5095	1.356774
•13307-01F	OK	7	0.2462445	0.003287	0.0098951	0	12.71848	2.17E-14	39.1%	100.0%	81.3076	49.74129	0.6654552
Integrated Age =												37	5
(•) Plateau Age =												**43.6**	**1.5**
Sample summary	ID	Irrad.	Material	Integ. Age	Error	% Rad	Age	Error	MSWD	Prob.	Steps	n/n-total	% Gas
Sample 5	13307	USGS8D	Groundmass	37	5	57.0	**43.6**	**1.5**	2.02	0.09	B,C,D,E,F	5/6	92.1
Sample 6													
13309-01A	OK	0.1	0.1610308	0.003605	0.1320008	0	21.5969	1.21E-14	15.4%	15.4%	35.6367	83.66899	4.653279
13309-01B	OK	0.3	0.1582823	0.0037996	0.0439438	0	15.75733	6.17E-15	7.9%	23.3%	54.8222	61.42584	1.983325
13309-01C	OK	0.6	0.1257438	0.0052413	0.0293573	0	13.39711	4.80E-15	6.1%	29.4%	60.6971	52.35725	1.684386
13309-01D	OK	1	0.1247051	0.0065339	0.0276672	0	12.66432	6.53E-15	8.3%	37.8%	60.7697	49.53235	1.446543
13309-01E	OK	3	0.1153233	0.0033103	0.0169894	0	13.85899	2.70E-14	34.5%	72.3%	73.4084	54.13551	0.9278719
13309-01F	OK	7	0.2473712	0.0059416	0.0067836	0	11.72146	2.17E-14	27.7%	100.0%	85.3967	45.89118	0.6316616
Integrated Age =												44	4
Approximate Age Range (no plateau) =												**40-50**	
Sample summary	ID	Irrad.	Material	Integ. Age	Error	% Rad	Age	Error	MSWD	Prob.	Steps	n/n-total	% Gas
Sample 6				13309	USGS8D	Groundmass	44	4	57.9	**40-50**	N/A	N/A	N/A

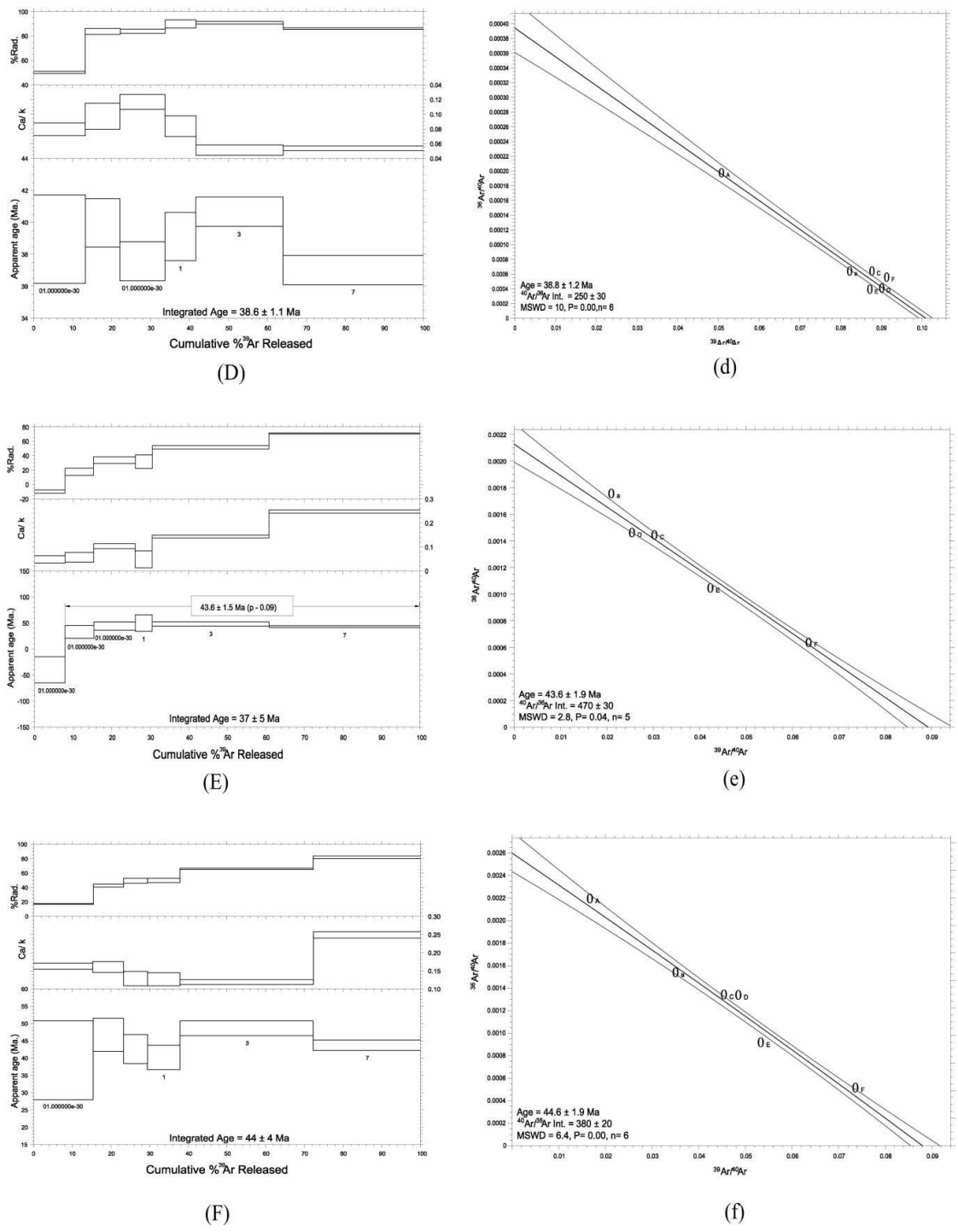

Fig. 3. The 40Ar/39Ar age spectra (A - F) and 36Ar/40Ar versus 39Ar/40Ar diagrams (a - f) of six metapelite samples from the Bulfat complex. A, a = Sample 1; B, b = Sample 2; C, c = Sample 3; D, d = Sample= 4; E, e = Sample 5; F, f = Sample 6

The nature of the discordance spectra of samples 4(35- 40 Ma) and 6 (40-50 Ma) may be related to the low initial $^{40}Ar/^{39}Ar$ value (259±30) in sample 4 and high initial 40Ar/36Ar value (380±20) in sample 6. Thus, various K –bearing mineral systems, i.e., mica and K –feldspar, especially in samples

4 and 6 may have been experienced a different diffusive loss of radiogenic argon and/or excess argon has been incorporated into marginal sites of these minerals as a result of reheating during the two stages of regional and contact metamorphisms. Plateau ages are commonly inferred to reflect the time of metamorphism and subsequent uplift and cooling history as well as intrusive age of the igneous body (Turner, 1970; Dallmeyer et al., 1981). In many instances, $40^{40}Ar/^{39}Ar$ dating is unlikely to provide the age of intrusion of the igneous body as the age typically marks the time when the minerals were cooled through their closure temperatures. The present K-bearing minerals, particularly biotite and muscovite, were recrystallized during the early stage of contact metamorphism at ~ 668 ^{o}C (Elias and Al-Jubory, 2013). The large difference between this proposed temperature and the presumed closure temperature for argon diffusion in biotite (300±50^{o}C) and muscovite (400±50 ^{o}C) (Jäger, 1979) leads us to interpret the timing (50–40 Ma) as the cooling period following the peak of the metamorphic event. This finding is an agreement with the 45 Ma cooling age (Jassim et al., 2006; Karim et al., 2015) of the Bulfat gabbro body.

Consequently, the intrusion of the igneous body and associated early high-grade thermal metamorphism may have probably taken place pre 50 Ma. In this concern, the late low grade thermal metamorphic event that occurred in conjunction with uplift, and cooling is characterized by crystallization of secondary muscovite that is difficult to be distinguished from primary muscovite by petrography investigation. Based on Mg –Fe exchange between biotite and muscovite, a possible temperature less than 580^{o}C (Elias and Al-Jubory, 2013) may refer to the late metamorphic event. Therefore, the most reliable estimate for the timing of late low grade thermal metamorphic event is ~30 Ma.

5. Conclusions

The present $^{40}Ar/^{39}Ar$ plateau age determinations of metapelitic rocks from Bulfat complex along Zagros Suture Zone, NE Iraq yielded between 32.9 and 50 Ma comprising ~ 58–100% of the ^{39}Ar released. Bulfat complex has experienced two metamorphic events: the first was regional (low – medium grade) occurred in the Iraqi Suture Zone during the period Albian–Cenomanian evident from 97-105 Ma K-Ar dating of hornblende separated from the spilitic diabase rocks of Mawat Ophiolite complex. This metamorphic activity was associated with the intraoceanic infant supra-subduction zone. The second was contact metamorphism (restricted mainly in Bulfat complex) due to the intrusion of mafic igneous body and overprinted the previous regional metamorphism pre 50 Ma ago. This igneous activity is regarded as one of multi-events magmatism that took place along Zagros Fold Thrust Belt (parallel to NW –SE) during the period from upper Cretaceous and Mid –Late Miocene, as a result of progressive plate convergence and closure of Neo –Tethys. In spite of the difference in time between the two metamorphic events by a value ~ 40 Ma., both were perhaps resulted from related to the two distinct subduction zones (Aziz, 1986). Evidence from the present 40Ar/39Ar dating of metapelites, and K –Ar dating of hornblende separated from the gabbroic body, suggest that the crustal rocks were subducted to the shallow depth and subjected to high-grade thermal metamorphism under conditions of hornblende to the onset of pyroxene hornfels facies (T = 668 C°, P = 2.9–3.5 kbar) pre - 50 Ma. Rocks were then influenced by cooling episodes during the period post 50–40 Ma (Lower – Mid Eocene). These rocks were later exhumed to upper crustal levels and probably suffered from low– medium grade metamorphism close to 30 Ma under conditions of albite–epidote facies (T = 581 C°, P= 2 kbar) due to crustal thickening that accompanied the increased rate of convergence between the Arabian Plate and the Iranian microplate. Consequently, we believe that the medium-high temperature, relatively low

–medium pressure thermal metamorphism slice of Bulfat Complex (Gemo–Qandil sequence) represents a part of the oceanic slab that has been subducted beneath Sanandaj–Sirjan Zone of Iranian microplate. This activity represents the last evolved episode of the island arc system ended with resorption of oceanic crust contemporaneous with the final closure of New –Tethys, and collision between the Arabian plate and Iranian microplate probably occurred at Mid –Late Miocene.

Acknowledgements

Analysis conducted by Dr. Hemming S. R, and Steven Cox from Department of Earth and Environment of Sciences, Columbia University (USA) are greatly appreciated. The authors would like to thank Drs.; Aswad and Al-Samman, Department of Geology, University of Mosul, for their assistance in sampling. The authors are very grateful to the reviewers, Editor in Chief Prof. Dr. Salih M. Awadh, the Secretary of Journal Mr. Samir R. Hijab, and the Technical Editors for their great efforts and valuable comments

References

Alavi, M., 2004. Regional stratigraphy of the Zagros fold-thrust belt of Iran and its proforeland evolution. American Journal of Science, 304, 1-20.

Aswad, K. J., 1999. Arc continental collision in Northeastern Iraq as evidence by the Mawat and Penjwen ophiolite complex. Rafidain Journal of Science, 10, 51-61.

Aswad, K.J., Al-Samman, A.H., Aziz, N.R., Koyi, A.M., 2014. The geochronology and petrogenesis of Walash volcanic rocks, Mawat nappes: constraints on the evolution of the northwestern Zagros suture zone, Kurdistan Region, Iraq. Arabian Journal Geoscience, 7 (4),1403-1432.

Aswad, K. J., Pashdary, M. A., 1984. Thermal metamorphism of impure carbonate xenoliths in the gabbroic rock of Bulfat complex, NE Iraq, Journal Geological Society of Iraq, 17, 208-235.

Aswad, K.J., Elias, E.M., 1988. Petrogenesis, geochemistry, and metamorphism of spiritized subvolcanic rocks of the Mawat Ophiolite Complex, NE Iraq., Ophiolite, 13, 95-109.

Aswad, K. J., Aziz, N. R., Koyi, H. A., 2011. Cr-spinel compositions in serpentinites and their implications for the petrotectonic history of the Zagros Suture Zone, Kurdistan Region, Iraq. Geological Magazine, 148 (5-6), 802–818

Aziz, N. R., 1986, Petrochemistry, Petrogenesis and Tectonic setting of Spilitic Rocks of Walash volcano-sedimentary group in Qala-diza area NE Iraq, Unpub. M. Sc. Thesis, University of Mosul, 181.

Aziz, N. R., 2008. Petrogenesis, Evolution and Tectonics of the Serpentinites of the Zagros Suture Zone, Kurdistan Region, NE Iraq. Unpublished PhD. Thesis, University of Sulaimani, Iraq, 250.

Aziz, N. R., Aswad, K. J., Koyi, H. A., 2011a. Contrasting settings of serpentinite bodies in the northwestern Zagros Suture Zone: Implications for the petrotectonic history of Zagros Suture Zone, Kurdistan Region, Iraq. Geological Magazine, 148 (5–6), 819- 837.

Dallmeyer, R. D., Odom, A. L., O'Driscoll, C. F., Hussey, E. M., 1981. Geochronology of the swift current granite and host volcanic rocks of the Love Cove Group, southwestern Avalon zone, Newfoundland: evidence of a late Proterozoic volcanic –subvolcanic. Association. Canadian Journal of Earth Science, 18, 699 –707.

Dalrymple, G. B., 1991. The Age of the Earth, California, Stanford University Press. 474.

Elias, M. E., Al-Jubory, Z. J., 2013. Provenance and tectonic setting of the metapelites deposits in the Bulat Complex, NE-Iraq. Arabian Journal of Geosciences, 7, 3589–3598.

Jäger, E., 1979. Introduction to geochronology. In: Lectures in Isotope Geology, Springer –Verlag. Berlin, 10, 1-12.

Jassim, S. Z., Buda, G., Neuzilova, M., Suk, M., 1983. Metamorphic development of the Iraqi Zagros Ophiolite Zone. Krystalinikum, 16, 21 –40.

Jassim, S. Z., Goff, J. C., 2006. Geology of Iraq. Published by Dolin, Prague and Moravian Museum, Brno, 16, 207.

Karim, K. H., Nabaz, R.H., Al-Bidary Mayssa A.A., 2015. Paragenesis and geochornological studies of Asnawa Iron Ore by the isotope and mineral chemistry in Penjween Area, Zagros Suture Zone Kurdistan Region, NE Iraq; Iranian Journal of Earth Sciences 7, 164-178.

McLennan, M., 1989. Rare earth elements in sedimentary rocks: Influence of provenance and sedimentary processes. Mineral, 21, 169–200.

Renne, P. R., Swisher, C. C., Deino, A. L., Darner, D. B., Owen, T. L., DePaolo, D. J., 1998. Intercalibration of standard absolute ages and uncertainties in 40Ar/39Ar dating. Chemical Geology, 145, 117-152.

Turner, G., 1970. 40Ar - 39Ar age determination of lunar rock 12013. Earth Planet Science Letters, 9, 177 –180.

Wijbrans, J. R., McDougall, I., 1988. Metamorphic evolution of the Attic Cycladic Metamorphic Belt on Naxos (Cyclades, Greece) utilizing 40Ar/39Ar age spectrum measurements. Journal metamorphic Geological, 6, 571–594.